# Squirrel Cage Rotor Design and Manufacturing for High-Speed Applications

Barta Jan, Uzhegov Nikita, Losak Petr, Ondrusek Cestmir, Mach Martin, Pyrhönen Juha



**DOI:** 10.1109/TIE.2018.2879285

# Squirrel Cage Rotor Design and Manufacturing for High-Speed Applications

Jan Barta, Nikita Uzhegov, *Member*, *IEEE*, Petr Losak, Cestmir Ondrusek, Martin Mach, and Juha Pyrhönen, *Senior Member*, *IEEE*

***Abstract*—A high-speed squirrel-cage induction machine requires a totally different design compared to the traditional squirrel cage industrial motor because of the mechanical limitations caused by the high speed. This results in a more complicated rotor construction and expensive material selection, and sets higher standards for the manufacturing precision. The objective of this paper is to demonstrate the design aspects, material selection, and manufacturing of a squirrel cage rotor for high-speed applications. In this paper, the rotor dimensioning approach based on equations and data analysis is presented. Rotor material selection and construction topology influence on the electrical machine design are discussed. The results are illustrated with the design of a 6 kW, 120 000 rpm induction machine for a turbo-circulator. The rotor parameters' influence on the electromagnetic performance of the designed machine is demonstrated. Mechanical stresses for different topologies are studied with Finite Element Method (FEM) analysis. Several manufacturing methods for producing a high precision rotor are described and compared. The presented rotor design approach, which enables high electromagnetic performance and robust construction, is verified by the testing of a prototype.**

***Index Terms*—AC machine, High-speed drive, Induction motor, Electrical design, Mechanical design, Manufacturing**

## I. Introduction

THE industry's need for high rotational speed electrical machines is based on several factors. First of all, in many application fields including microturbines, machining tools, compressors, and vacuum pumps higher rotational speeds increase process efficiency. High-speed electrical machines enable a direct connection between the machine and the working tool increasing system efficiency. Other benefits include a smaller size, and reduced material consumption of the high-speed electrical machine compared with the conventional machines [1], [2]. There is also higher efficiency for partial loads because the wide speed range is a significant advantage in various industrial applications.

The current trend in scientific publications shows that permanent magnet synchronous machines are usually preferred for high-speed applications [3], [4]. The advantage of synchronous machines is their high efficiency and power factor compared with induction machines [5]–[7]. Despite this, the induction machines have their advantages, especially resistance to high temperatures, lower manufacturing costs, simpler control, and if a solid rotor is used, they can tolerate high mechanical stresses [8], [9].

The following rotor solutions for a high-speed induction machine are mainly used: smooth solid rotor structure, slitted solid rotor structure, coated rotor structure, and caged rotor structure. Comparisons show that the best electromagnetic parameters can be achieved by a properly designed induction machine with a squirrel cage rotor [10], [11]. This machine has a smaller slip, higher efficiency, and higher power factor compared with the other solid rotor alternatives. It is used for industrial low- and medium-speed applications. On the contrary, the overview of the rotor topologies presented in [12] and [13] shows that a squirrel cage rotor is not preferred when it comes to high-speed applications. This is because a squirrel cage rotor is challenging and complicated in several aspects at high speeds. The rotor itself is exposed to high frequencies, centrifugal forces, dynamic bending and high temperatures during the operation [14]. Other mentioned rotor topologies may be more resistant to these effects.

A multi-domain design procedure for high-speed machines is described in [15]. The researchers show how to design a machine from the electromagnetic, thermal, and mechanical points of view. For the machine dimensioning, it is suggested to use classical equations based on knowledge of mechanical machine constants. However, recommended values of mechanical machine constants for high-speed machines are not given. More practical data for the dimensioning of high-speed machines are given in [16] and [17]. Unfortunately, the presented values of the mechanical machine constant are only for a limited number and range of high-speed induction machines. Other suitable data for the dimensioning of high-speed machines is limited.

A comprehensive design, including a manufacturing description of a 21 kW, 50 000 rpm high-speed induction machine with a squirrel cage rotor has been done in [18]. The

This research work has been carried out in the Centre for Research and Utilization of Renewable Energy (CVVOZE). Authors gratefully acknowledge financial support from the Ministry of Education, Youth and Sports of the Czech Republic under NPU I programme (project No. LO1210)

Jan Barta, Cestmir Ondrusek and Martin Mach are with Department of Power Electrical and Electronic Engineering, Brno University of Technology, 616 00 Brno, Czech Republic (e-mail: bartaj@feec.vutbr.cz, ondrusek@feec.vutbr.cz, machm@feec.vutbr.cz).

Nikita Uzhegov is with SpinDrive, Lappeenranta, Finland (e-mail: nikita.uzhegov@spindrive.fi).

Petr Losak is with Institute of Solid Mechanics, Mechatronics and Biomechanics, Brno University of Technology, 616 00 Brno, Czech Republic (e-mail: losak@fme.vutbr.cz)

Juha Pyrhönen is with the Department of Electrical Engineering, School of Energy Systems, LUT, Lappeenranta, Finland (e-mail: juha.pyrhonen@lut.fi).

paper discusses the electromagnetic and mechanical design of the machine. However, the electromagnetic design was based on conventional induction machines, and the rotor was built with a structure designed for low- and medium-speed machines. The rotor was assembled by torch brazing. Other examples of the design of high-speed induction machines with squirrel cage rotors can be found in [19]–[21]. In all these publications, conventional rotor structures are implemented. The provided mechanical designs mainly concentrate on the analysis of rotor stress in the active magnetic part.

The most critical part of a squirrel cage rotor is the short-circuit ring [22]. To overcome its mechanical limitations, and extend the speed range of the machine, the short-circuit ring must be designed differently compared to the traditional one. This topic was studied in [23] and [24]. Although the authors provided a feasible solution for a high-speed squirrel cage rotor, no comparison of the different solutions was given.

The main contribution of this paper is the design and manufacturing guidelines for a squirrel cage rotor suitable for high-speed applications. The recommended values of the mechanical machine constant and tangential stress based on industrial experience are identified. The rotor design is aimed to maximize the electromagnetic performance and ensure stable operation at high speeds. Different rotor topology solutions for high-speed machines, and their manufacturing processes, are described and compared. Rotor material selection is an important part of this study. The case study of a 120 000 rpm, 6 kW induction machine illustrates the presented design approach. The results of this study are verified by prototype measurements.

## II. Rotor design aspects

### A. Rotor dimensioning

The selection of the main machine dimensions is the first design challenge. The main dimensions are referred to as the outer diameter of the rotor and its length. The main dimensions are often selected based on experience from previous designs, or on empirical recommended ranges. For low- and medium-speed machines, the recommended values can be found in the literature. These values are dependent on the electromagnetic load of the machine, which is usually expressed by the flux density and current density. The maximum values of these variables are constant, and are caused by the saturation of magnetic materials and the allowed temperature rise of the machine. The machine load is closely related to the losses, which together with cooling determine the upper limit for the continuous power that can be obtained from a given machine volume. The dimensions of the rotor can be determined based on the knowledge of the mechanical machine constant, $C_{\mathrm{mec}}$ [25]. This constant was firstly defined by Engelbert Arnold at the beginning of the 20th century and, therefore, it is also called Arnold's constant. This constant is defined as follows:

$$C_{\mathrm{mec}} = \frac{P}{D^2 l n_{\mathrm{syn}}}, \tag{1}$$

where $P$ is the output power of the machine, $D$ is the rotor outer diameter, $l$ is the rotor length, and $n_{\mathrm{syn}}$ is the rotor synchronous speed. The mechanical machine constants of well-designed machines are empirical knowledge obtained from previously produced electric motors of the given type and power. The dependence of the electrical machine constant on power in the range from 2 kW to 1000 kW for totally enclosed, low-speed motors with one pole pair, $p = 1$, is shown by the curve in Fig. 1(a). High-speed machines have a significantly higher loss density than the conventional ones. Therefore, a more efficient cooling is required. In high-speed machines, the level of linear current density and air-gap flux density is also different. The choice of their main dimensions must meet the electromagnetic, mechanical, and thermal requirements. High-speed machines often operate at the limit of these requirements. In many cases, the nominal operating speed of the machine should be below the first critical speed with a sufficient margin. This enables undercritical operation and allows the use of various bearing types. However, overcritical operation is also possible using, for example, active magnetic bearings. The selected outer diameter of the rotor significantly affects the centrifugal forces, which the rotor must tolerate. The length of the rotor must meet the rotordynamics requirements. All these facts mean that the curve shown in Fig. 1(a) should not be used when designing a high-speed machine.

Research into already implemented machines was carried out in the first stage. The basic dimensions of the elements for a high-speed machine can be found in the catalogs of their manufacturers. In this work, the catalog data [26]–[28] were used for the determination of a mechanical machine constant for 447 machines. The mechanical machine constants were calculated using (1) and are plotted in Fig. 1(a). The plotted data are for high-speed solid rotor induction machines with a squirrel cage rotor. The cooling of these machines is arranged by using the water flow through a helictical channel located in the stator frame. Such a cooling arrangement corresponds to a water-jacket cooling system.

The stated values of the constants are from 50% to 90% of the mechanical machine constants specified in [25] for conventional totally enclosed induction machines. It is obvious that the mechanical machine constant of high-speed machines grows with the increase of the output power in a similar way to standard machines.

Another approach for determining rotor dimensions is by selecting the torque per rotor volume constant (TRV). This constant is defined by the following equation:

$$TRV = \frac{T}{V_{\mathrm{r}}}, \tag{2}$$

here $T$ is the torque and $V_{\mathrm{r}}$ is the rotor volume. Typical values of TRV for conventional electrical machines are shown in [29]. For the high-speed electrical machines shown in Fig. 1(a), the TRV is determined and is shown in Fig. 1(b). It can be seen that a higher TRV is applied for a lower speed range and higher power whereas a lower TRV is applied for a higher speed range and lower power. For the majority of the speeds studied, the TRV dependency on power is close to a linear function.

Torque per rotor volume is related to the tangential stress acting on the surface of the rotor. The tangential stress, $\sigma_{\mathrm{Ftan}}$

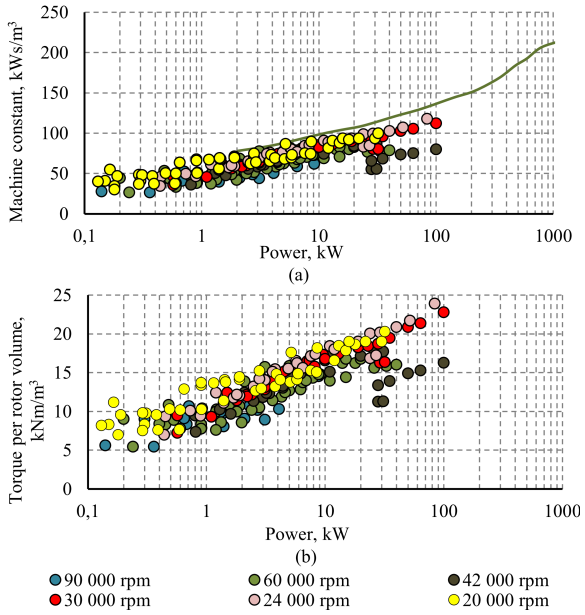


Fig. 1: (a) Machine constants (the green line is a mechanical machine constant of totally enclosed asynchronous machines reproduced from [25]) and (b) torque per rotor volume, for the water-jacked-cooled solid-rotor high-speed induction machines with a squirrel cage rotor.

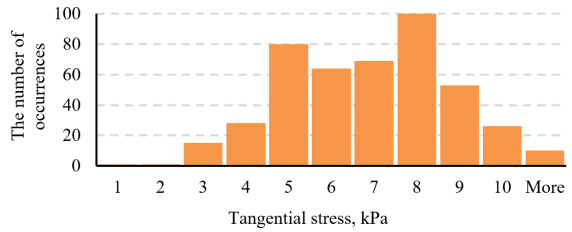


Fig. 2: Tangential stresses for the water-cooled solid rotor high-speed induction machines with a squirrel cage rotor.

can be calculated using the following equation:

$$\sigma_{\mathrm{Ftan}} = \frac{TRV}{2}. \tag{3}$$

The publication [25] indicates that the tangential stresses for conventional induction machines should vary between 12 kPa and 33 kPa. For the high-speed electrical machines shown in Fig. 1, the tangential stress on the rotor surface was determined. The results are shown in the histogram in Fig. 2. Only 10 out of the 447 computed machines had a tangential stress higher than 10 kPa. Lower tangential stresses of solid-rotor high-speed induction machines can be explained by their higher loss density. Therefore, it is more difficult to cool down the machine, and lower tangential stresses are allowed. This also indicates that water-jacket cooling is not a very efficient way of cooling high-speed motors where efficient forced ventilation may allow higher tangential stress values.

The main dimensions of the high-speed machine can be selected in accordance to the data presented in Figs. 1 and 2. Together with the main dimension selection, the materials implemented in the machine must be appropriately chosen. The selected materials determine the mechanical strength of the rotor, and its losses. In order to ensure the mechanical strength of the rotor at high speeds, it is necessary to design a rotor structure in a different way compared with the low- and medium-speed constructions.

### B. Rotor materials

In most cases, a squirrel cage rotor consists of two materials. The first one is used for the squirrel cage itself. This material must have a high conductivity. The second is the material for the rotor body, which must have good electromagnetic properties, which means high saturation flux density, low hysteresis, and high resistivity. In addition to these material property demands, there is a requirement for high mechanical strength in high-speed machines. For a certain surface speed of the rotor, the rotor cannot be made from the materials that are typical for the low- and medium-speed machines. Materials should keep their mechanical properties even at very high temperatures. This is important during operation of the machine, and especially during the rotor fabrication, when the rotor materials can be exposed to even higher temperatures.

In a squirrel cage, the use of ordinary copper is often not possible. After thermal treatment, ordinary copper loses its already low mechanical yield strength. Therefore, alternative materials are used in high-speed machines with squirrel cage rotors. An alternative solution for the high-speed induction machines is the use of Glidcop family materials [12], [18], and [30]. Another option is beryllium alloys, which can tolerate high stresses, but have significantly lower conductivity than copper [23]. Another disadvantage is the toxicity of beryllium, which is a problem in terms of production.

From the electromagnetic point of view, it is always preferable to use a laminated rotor core, which limits the core losses significantly. Induction machines with a laminated rotor core reach higher efficiency compared with those with solid rotor cores. Suitable materials for laminated cores in high-speed machines are listed in [12]. The 10JNEX900 and 10JNF600 lamination steels have high values of mechanical strength. High-speed machine designs with laminated rotor cores are reported in [31] and [32].

However, a laminated rotor core is not suitable for the highest rotor surface speeds. The bending stiffness of the laminated rotor is smaller compared with the solid rotor. Reduced stiffness leads to a decrease in critical speed which is undesirable for high-speed machines. In the case study machine, even with a solid rotor the safety margin to the first bending mode was close to the critical value. Therefore, the solid rotor core is selected for the more demanding cases. For example, the commonly available grades of 41CrAlMo7, 41CrMo4, and S355J can be implemented. For more demanding applications, it is possible to use steel from the AerMet and Marage families, which were originally developed for military aircraft applications [33]. AerMet steel was used to build a high-speed machine in [30].

The final selection of the core material should take into account the rotor surface speed and associated mechanical stresses. Higher rotor surface speed may require the selection of a solid rotor core, and cage materials with a higher yield strength. This often results in lower conductivity, which is

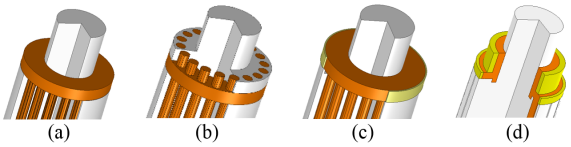


Fig. 3: Rotor topology options for high-speed applications: (a) conventional (topology A); (b) with supporting ring (topology B); (c) with reinforcement ring (topology C); (d) with modified shape and reinforcement ring (topology D).

actually a benefit for the core, but not for the cage. As a result, in some applications, it may be beneficial to operate an induction machine at a lower peripheral speed that would allow implementation of the laminated rotor. These factors should be considered at the very beginning of the design stage.

### C. Rotor topology for high-speed applications

Dimensions of the rotor, together with the selected materials, define the rotor rotation limit. The mechanical safety factor, however, can be increased by selecting an appropriate rotor topology. A rotor topology for low- and medium-speed induction machines is shown in Fig. 3(a). This topology is referred to as topology A. Topology A is sometimes used in high-speed applications [18]. The generated stress inside the rotor can be decreased by appropriate shaping of the short-circuit rings. This can be achieved by concentrating most of the short-circuit ring volume in a lower radius. As a result, the mechanical stresses in the short-circuit rings are reduced. A similar solution for higher rotor mechanical strength is shown in [23] and [34].

For high-speed applications, shaping the short-circuit rings may not be enough to keep the required safety factor. The next way to increase the rotor rigidity is by supporting the rotor structure. As the most critical part from the mechanical point of view is the short-circuit ring, this part must be reinforced. The first approach for doing this is placing a supporting ring next to the short-circuit ring, as is shown in Fig. 3(b). The supporting ring should preferably be made from non-magnetic material, otherwise it would increase the leakage inductance of the short-circuit ring. This topology is referred to as a topology B. The second approach is a shrink fitting of the reinforcement ring on the short-circuit ring, as shown in Fig. 3(c). The material of the reinforcement ring may be, for example, titanium or carbon fiber. This topology is referred to as topology C and similar design approach of the rotor has been shown in [24] and [35].

By combining the reinforcement methods mentioned above, another rotor topology can be developed. A combination of the appropriate rotor shaping for topology A with a shrink fitted reinforced ring from the topology C can result in the topology developed for the case study rotor shown in Fig. 3(d). This topology combines the advantages of both short-circuit ring stress reduction techniques.

The rotor topology selection significantly affects the manufacturing complexity and the maximum tolerable surface speed of the rotor. More comprehensive description of topologies suitable for use in high-speed cage induction machines was given in [36]. In this paper, referred topologies are studied and compared in more detail in Section III-C.

TABLE I: Case study machine key parameters.

| Parameter | Value |
|---|---|
| Pole pairs | 1 |
| Nominal frequency, Hz | 2015 |
| Voltage supply, V | 350 |
| Connection | Star |
| Number of stator slots | 12 |
| Number of rotor slots | 18 |
| Active length, mm | 50 |
| Stator outer diameter, mm | 90 |
| Rotor outer diameter, mm | 30.7 |
| Rotor surface speed, m/s | 193 |
| Mechanical machine constant, kWs/m$^3$ | 66.67 |
| Tangential stress, kPa | 6.44 |

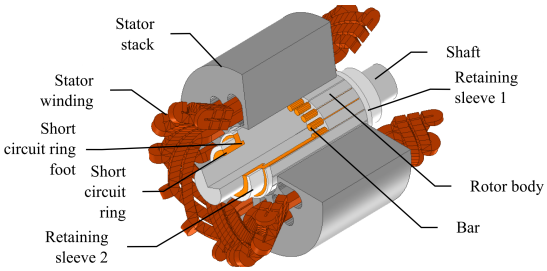


Fig. 4: Model of the 6 kW, 120 000 rpm induction machine with a squirrel cage rotor.

## III. Case Study

### A. Case study description

As a case study, a high-speed induction machine with a squirrel cage rotor was designed for a helium turbo-circulator. The targeted turbo-circulator requires a motor with an output power of 6 kW at 120 000 rpm [37]. This is a challenging application in terms of the speed range and mechanical stresses for a squirrel cage rotor. This type of construction has been selected to illustrate how to expand the limits of this rotor topology.

The induction machine has two poles with distributed double-layer short pitched winding located in 12 stator slots. The rotor surface nominal peripheral speed is 193 m/s. The main dimensions of the rotor were selected based on the research results presented in Section II-A. The selected mechanical machine constant equals 66.67 kWs/m$^3$. It can be seen in Fig. 1 that the mechanical machine constant for a certain power decreases with increasing rotational speed. Therefore, the selected value of the mechanical machine constant for the designed 120 000 rpm machine is lower than the mechanical machine constants calculated for 90 000 rpm. The cooling method has also affected the value of the mechanical machine constant. Tangential stress for the determined rotor volume and required torque is 6.44 kPa, which corresponds well with the data in Fig. 2. More details about the multidisciplinary design process of the case study machine can be found in [22]. A model of the designed machine is shown in Fig. 4, and its key parameters are listed in Table I.

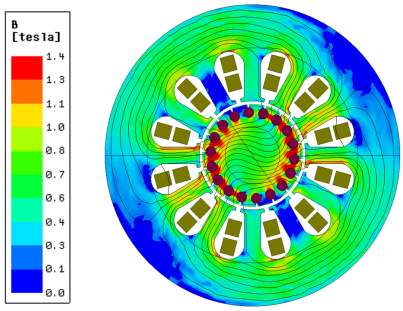


Fig. 5: Magnetic flux distribution at the rated operating point.

TABLE II: Case study machine electromagnetic losses at the nominal load.

| | Stator core, W | Stator winding, W | Rotor bars, W | Solid rotor, W |
|---|---|---|---|---|
| Value | 299 | 150 | 62 | 72 |

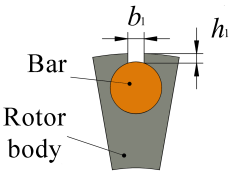


Fig. 6: Rotor slot and the main dimensions of the slot opening.

The electromagnetic calculation of the case study machine was made in Ansys Maxwell software. The calculated flux density distribution for a rated operating point is shown in Fig. 5. For reduction of the core losses, the flux density level is kept below 1 T inside the stator yoke. This is achieved by increasing the stator yoke thickness. The rotor is magnetically saturated between and below the rotor bars causing additional losses in excitation.

All calculated electromagnetic loss components are listed in Table II. Losses in the solid rotor body were higher compared with the rotor bar losses. These losses were mainly a result of the high-frequency variation in the air-gap flux because of the slotting.

### B. Rotor design for optimal electromagnetic performance

As shown below, for an optimal electromagnetic performance of the caged solid rotor, it is beneficial to have semiclosed rotor slots. Such slots reduce the rotor leakage inductance, which results in lower slip. For the machine designed, the rotor slot opening width $b_1$ and the rotor slot opening height $h_1$ shown in Fig. 6 were studied to increase the electromagnetic performance.

The optimization results from the finite element analysis are shown in Fig. 7. The analysis demonstrates that even a narrow slot opening in the rotor slot has a significant impact on the improvement of the machine performance.

Machine performance drops steeply when the rotor slot opening width is below 0.1 mm. Over this value, the performance of the machine is almost constant in the observed range. An increase in the slot opening height $h_1$ results in lower machine performance. However, the effect is minimal when

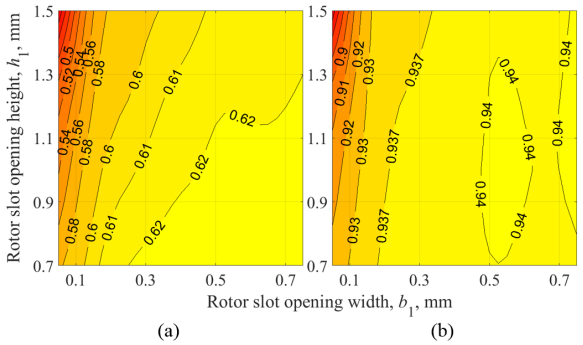


Fig. 7: (a) Power factor map, and (b) efficiency map, for various slot opening widths and heights.

considering the design area, where the slot opening width is above 0.1 mm.

From the mechanical point of view, it is preferable to have bars located deeper under the rotor surface. Stress distribution in the rotor slot area is demonstrated in Section III-C. The rotor slot openings make a deeper location of the rotor bars possible. This solution also provides a better electromagnetic performance compared with the closed rotor slot option. Rotor slot openings are, therefore, of great practical importance in the design of the high-speed squirrel cage rotor.

### C. Rotor mechanical design

The rotor topologies presented in Section II-C are investigated to study their influence on the rotors mechanical limits. This mechanical analysis was conducted using 3D FEM. To ensure a fair comparison, the cross-section of the end-ring for all options is kept the same. The rotor temperature was selected at 200 °C for the whole volume.

As the mechanical properties of squirrel cage rotors are very sensitive to the clearances between the individual parts, partial optimization was performed for each of the compared options. Therefore, the mechanical tolerances of the inner diameter of the rotor, the diameter of the bars, the overlap between the bars and short-circuit rings, the overlap between the titanium retaining ring and short circuit ring, and the titanium retaining ring thickness were optimized. The screening optimization method implemented in Ansys Mechanical software was used. This method is suitable for the preliminary design. The goal of the optimization was to minimize the stresses in all rotor parts with equal importance. A yield strength valid at room temperature was used for the safety factor estimation. The manufacturer did not provide temperature-dependent material characteristics. The safety factors for optimized geometries are shown in Table III. In this table, the best-achieved values are highlighted in green, and the least favorable are highlighted in red. The von-Mises stress distribution in the rotor is shown separately for each topology in Fig. 8. The resultant stress was due to centrifugal forces and stress produced by the different thermal expansions of the individual materials. The analysis results show that the rotor bars have the highest safety factor in the rotor structure, excluding the safety factor of the shaft, which is not considered in the analysis. Short-circuit rings

TABLE III: Results of the mechanical analysis for different rotor topology options.

| Part | Material | Yield strength, MPa | Safety factor | | | |
|---|---|---|---|---|---|---|
| | | | Top. A | Top. B | Top. C | Top. D |
| Bars | Glidcop® | 469 | 2.19 | 2.32 | 3.45 | 2.76 |
| End-ring | AL-15 | 455 | 1.16 | 1.12 | 1.76 | 1.78 |
| Rotor body | 41CrMo4 | 760 | 1.55 | 1.52 | 1.34 | 1.46 |
| Reinforcement ring | | | - | 1.34 | - | - |
| Retaining sleeve 1 | TiAl6V4 | 1000 | - | - | 1.50 | 1.54 |
| Retaining sleeve 2 | | | - | - | - | 1.63 |

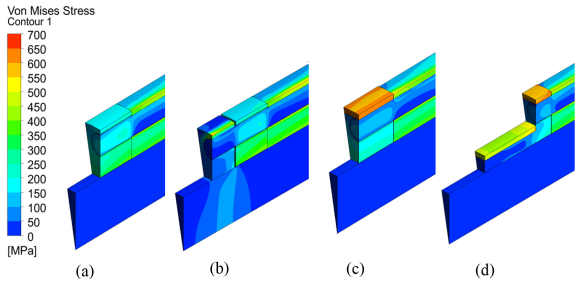


Fig. 8: Von-Mises stress distribution in different rotor topology options: (a) topology A; (b) topology B; (c) topology C; (d) topology D.

and the rotor body are the most critical components from the mechanical point of view.

Topology D has the highest safety factors for the critical rotor components among the topologies analyzed. The final rotor dimensions were calculated by a multidisciplinary design approach, which has changed some parameters compared with topology D. This is because the connection of the bars to the ring is ensured by strict manufacturing tolerances and pressed joints, and are not soldered. The final rotor construction is shown in Fig. 9. The final dimensions were optimized by using a genetic algorithm. The goal was to ensure that the rotor would tolerate the centrifugal forces in a wide temperature range. Unlike topology D, this rotor also has a so-called foot towards the rotor body, as shown in Fig. 4. This foot helps in the rotor assembly process, and partially contributes to the short-circuit ring stress relief.

The results of the mechanical calculation for the rotor intended for manufacturing are shown in Fig 9. These results are for the case of shrink fit rotor assembly after the dimension optimization. Because of the shrink fit assembly, the stresses are higher in some rotor parts compared with the results from Fig. 8(d). Stresses in the rotor body slot area are shown in Figs. 9(c) and (d). The maximum stresses of 681 MPa and 669 MPa for 20 °C and 200 °C respectively occur at the bottom of the slot. Since the von-Mises stress is below the yield strength, no plastic strain occurs in the rotor body slot area. The short-circuit ring is the part with the lowest safety factor, and it is the most critical part of the entire rotor structure from the mechanical point of view. The distribution of the safety factor inside the short-circuit ring is shown in Figs. 9(e) and (f) for 20 °C and 200 °C, respectively. The red areas have safety factors below one. It is assumed that local plastic deformation will occur in these places without affecting the overall strength of the rotor. Growth of the plastic strain is limited by the retaining ring.

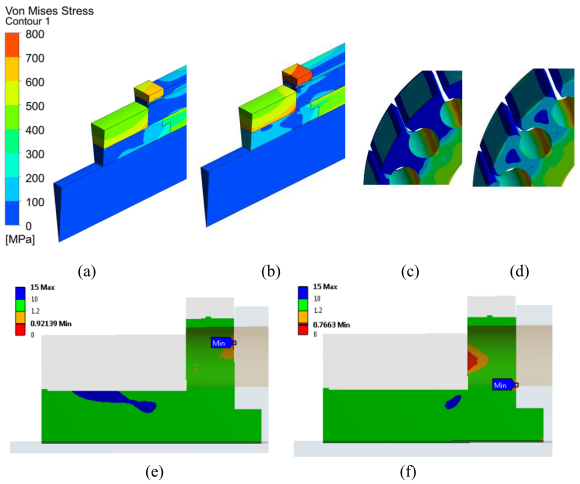


Fig. 9: Results of the mechanical analysis for the final rotor design: (a) Von-Mises stress distribution at 20 °C; (b) Von-Mises stress distribution at 200 °C; (c) Von-Mises stress distribution for the bar hole inside the rotor at 20 °C; (d) Von-Mises stress distribution for the bar hole inside the rotor at 200 °C; (e) safety factor distribution in the short-circuit ring at 20 °C; (f) safety factor distribution in the short-circuit ring at 200 °C.

The von-Mises stress distribution in the final rotor is shown for 20 °C in Fig. 9(a), and for 200 °C in Fig. 9(b). The rotor bars have the lowest stresses and the highest safety factor in the entire rotor structure. The reinforcement rings have the highest stresses. Their safety factor ranges from 1.15 to 1.28. The rotor body is also subjected to high stresses, and its safety factor is from 1.12 to 1.14. All these values are remarkably low, and no big errors in the design work are allowed.

The results of a large number of FEM simulations have shown that all rotor part stresses are highly dependent on the manufacturing tolerances. This puts high demand on the precise manufacturing and assembly of the rotor. For example, the rotor bars must be made with a diameter tolerance between 0 and 4 $\mu$m.

The next step in the mechanical design is a detailed analysis of the rotordynamics since the dimensions and characteristics of the rotor and the bearings were known. For the rotordynamic analysis, the 2D finite element method was used. The first bending occurs at a critical speed of 175 000 rpm.

## IV. Manufacturing

The manufacturing process and tolerances are critical factors that influence the mechanical rigidity of the rotor at the same level as the material selection or rotor dimensioning. Several different approaches were investigated:

- Electron beam welding. The maximum depth of penetration was about 3 mm.
- Vacuum brazing with brazing alloy Ag72Cu. The brazing alloy diffused into the Glidcop Al-15 volume, and no joint was formed.
- Vacuum brazing with Ag72Cu brazing alloy with a nickel layer. The nickel layer was formed by chemical nickel plating. According to the data on Glidcop Al-15, the chemical layer is porous, and the diffusion brake is inadequate. Connections were not created.

Fig. 10: The rotor elements for brazing assembly and the rotor after brazing

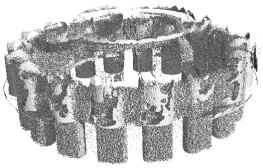

Fig. 11: CT scan results for one end of the brazed rotor. The joints are porous.

- Brazing with an air gas burner and Ag55Sn brazing alloy. The connections on the simplified samples were successful, and fulfilled the requirements for their quality.
- Shrink fit assembly.

Among the manufacturing processes tested, only two have shown promising results. This section describes the results obtained by brazing with an air gas burner and shrink fit assembly.

### A. Brazing

A simplified rotor model was produced to verify the successful preliminary brazing results. A simplified rotor model was made according to topology A shown in Fig. 3(a). Rotor parts were placed on an expansion mandrel. This mandrel served to fix the rotor components in the desired positions during soldering.

Brazing of material Glidcop was performed by using Ag55Sn brazing alloy with a brazing temperature of around $670\,^{\circ}\mathrm{C}$. All rotor components were heated approximately to this temperature during the process which takes a few minutes; therefore, the mechanical stiffness of the components may decrease. This weakening of the rotor components because of the heating can potentially cause the machine to malfunction.

The rotor after the brazing process and its elements are shown in Fig. 10. It was difficult to heat the rotor components to form a connection using the brazing alloy. The brazing alloy also created an undesirable rigid joint between the mandrel and the rotor. It was necessary to drill the mandrel due to the nature of this connection.

To investigate the quality of the assembly, industrial computed tomography (CT) scanning was performed on one end of the rotor. The results are shown in Fig. 11. This figure shows a 3D visualization where the brazing alloy is located. The brazing alloy can be seen as a solid silver layer. The dotted points are related to the bars and the short-circuit ring. It can be seen that the brazing alloy does not fill the entire space between the bar and the short-circuit ring. The different bars have different qualities of this connection. Such a connection of the individual bars with the short-circuit ring may also have different resistance. The mechanical properties of the individual joints may also vary.

The assembly of the rotor by brazing thus proved to be unreliable. Even after a large series of the sample tests, the required connection quality was not achieved on the real rotor. The brazing assembly option was not successful, and requires additional investigation.

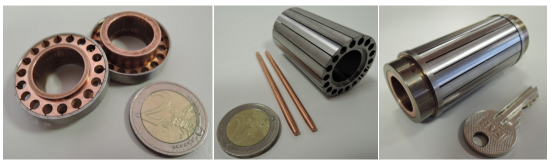

Fig. 12: The rotor elements for shrink fit assembly and completed rotor.

### B. Shrink fit assembly

The advantage of shrink fitting is that there is no brazing alloy, and the material heating is limited and can be controlled compared with brazing. This significantly reduces the risk of changes in the material properties. The disadvantage of this approach is the high demands set for the manufacturing tolerances of each rotor part. The shrink fit procedure for the proposed rotor construction can be summarized into four steps:

1) Shrink fitting of the retaining sleeve on the short-circuit ring before making the holes for the bars. The short-circuit ring was cooled in liquid nitrogen, and the retaining sleeve was preheated in hot air to $250\,^{\circ}\mathrm{C}$.
2) Shrink fitting of the bars into the short-circuit ring. The bars were cooled in liquid nitrogen, and the short-circuit ring was preheated in hot air to $250\,^{\circ}\mathrm{C}$. To simplify the assembly process, the diameter of the ends of the bars should gradually decrease.
3) Shrink fitting of the smaller retaining sleeve on the short-circuit ring. The rotor assembly was cooled, and the smaller retaining sleeve was preheated in hot air to $250\,^{\circ}\mathrm{C}$.
4) Shrink fitting of the rotor on the shaft. The shaft was frozen to $-200\,^{\circ}\mathrm{C}$, and the rotor was heated to $300\,^{\circ}\mathrm{C}$.

The most complicated part of the process was guiding the parts towards each other during the assembly. Shrink fitting must be completed quickly to avoid temperature equalization. The centering guidance elements on the assembly parts can significantly simplify this process. The elements and the successfully assembled rotor are shown in Fig. 12. This rotor is implemented in the induction machine for a helium turbo-circulator.

## V. Testing

The rotor was balanced after the shrink fit assembly process. Balancing was made for the complete rotor equipped with an axial bearing disk and the impeller. Together with the designed stator, the rotor was used to assemble the turbo-circulator. The turbo-circulator without volute and its elements can be seen in Fig. 13. For the turbo-circulator, tilting pad journal bearings with pads supported on elastic elements were used. To evaluate the electrical machine design, testing was performed.

### A. Test Installation

The installation for testing the turbo-circulator without compressor housing is shown in Fig. 14(a). The frequency

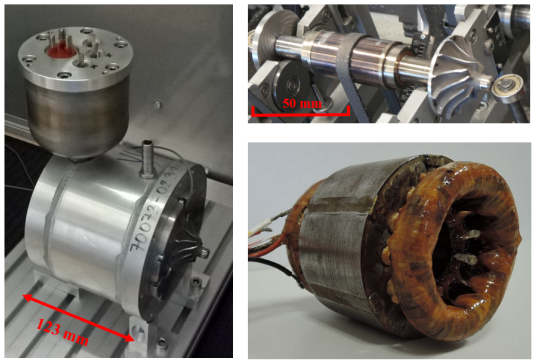


Fig. 13: Assembled compressor, rotor during balancing and the wound stator.

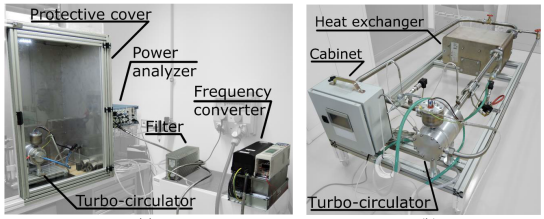


(a) (b)

Fig. 14: Test installation for the measurements of the turbo-circulator: (a) without a compressor housing; (b) under load condition.

converter used to drive the machine is shown on the right side. The power analyzer Yokogawa WT1800 was used for the measurements which were performed with a filter so as to suppress the higher harmonic components of the supply source.

For testing the turbo-circulator under load condition, the test bench was manufactured and is shown in Fig. 14(b). It consisted of a closed air-circuit for loading the machine; air was used instead of helium, for simplicity, and the output power of the machine was regulated by pressurizing the air. Both air pressure and temperature were measured in the inlet, outlet, and by-pass of the turbo-circulator. These data were post-processed and used for calculating the machine's output power by way of a programmable logic controller located inside the cabinet. The temperature of the stator windings and vibrations of the compressor housing were also measured.

### B. Test without compressor housing

Turbo-circulator measurements without compressor housing were made to verify bearing and electrical machine behavior up to a rated operating speed. It was not possible to run the motor at no-load because of the attached impeller. Removal of the impeller was not possible because the rotor was balanced with it. During testing, the rotor was rotating up to the nominal speed. The dependency of the input power on the supply frequency is shown in Fig.15(a).

During this test, relative rotor displacement was also measured. For this purpose, two inductive sensors were used. The first sensor was placed behind the impeller and the second one fixed to the axial bearing for measuring the deflection of the axial bearing disk. The measured data is shown in Fig. 15(b) which demonstrates that the relative rotor displacement amplitude at both ends of the rotor was relatively low. Displacement

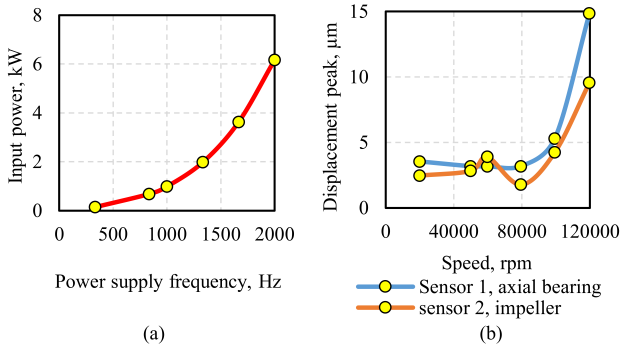


(a) (b)

Fig. 15: Measured: (a) motor input power as a function of supply frequency; (b) rotor displacement peak as a function of rotation speed.

did not exceed 5.3 $\mu$m up to a rotor speed of 100 000 rpm. At speeds above this, however, both rotor ends' displacement increased significantly: 9.5 $\mu$m at 120 000 rpm on the impeller side and 14.9 $\mu$m on the axial bearing disk side. The maximum allowable relative displacement amplitude was 7.5 $\mu$m for the continuous operation of the designed machine construction.

The measured data shows that the turbo-circulator could not operated safely at its nominal operating speed of 120 000 rpm. However, this test also demonstrated that the rotor was capable of operation at its rated speed from a mechanical perspective since it can tolerate centrifugal forces. Thus, approach to the mechanical design of the rotor and its manufacturing are verified. The origin of this significant displacement might be non-compliance with manufacturing tolerances, incorrect input data of the bearing stiffness and damping for rotordynamic calculation, movement of the shrink-fitted parts during the operation, etc.

### C. Test under load conditions

Due to the detected problems with the rotordynamics, the verification of the electromagnetic performance was limited to a supply frequency of 1666 Hz only which corresponded to a synchronous speed of 100 000 rpm. The selected speed was safe from an operational point of view with respect to the relative rotor displacement shown in Fig. 15(b). The loading of the machine was gradually increased by pressurizing the air in the pipelines. The maximum value measured for the turbo-circulator inlet pressure was 2.4 bar with an outlet pressure of 3.4 bar. At this pressure, the air flow was 95 g/s. It was not possible to load the machine further at the constructed test bench because of the aerodynamic limitation of the pipelines. The derived efficiency and power factor of the turbo-circulator are shown in Fig. 16.

Three points with an output power of 1.9, 3 and 4.1 kW were selected for a comparison with a finite element model shown in Section III-A. The actual pressure and temperature measurements for selected powers are shown in Table IV. The measured and calculated data are compared in Table V. The electromagnetic model was set up to have the same line-to-line voltage and frequency as a tested machine during the measurements. The rotational speed in the FEA model was varied to match the measured input power and then the electromagnetic losses were estimated. Unfortunately, it

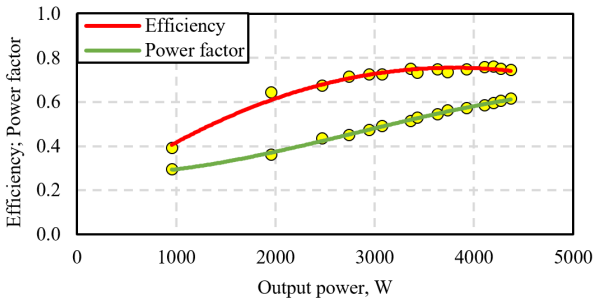


Fig. 16: Efficiency and power factor of the turbo-circulator as a function of an output power of 100 000 rpm.

TABLE IV: Pressure and temperature measurements for selected mechanical powers.

| Output power, W | Inlet pressure, bar | Outlet pressure, bar | Inlet temperature, °C | Outlet temperature, °C | Stator winding temperature, °C |
|---|---|---|---|---|---|
| 1955 | 1.20 | 1.66 | 25.6 | 61.3 | 41.5 |
| 3075 | 1.80 | 2.53 | 25.1 | 65.7 | 64.8 |
| 4110 | 2.40 | 3.37 | 24.7 | 66.8 | 77.7 |

TABLE V: Comparison of the selected measured and calculated data.

| Output power, W | Line-to-line voltage, V | Input power, W | Current, A | | Power factor | | FEA Losses, W | | |
|---|---|---|---|---|---|---|---|---|---|
| | | | Measured | FEA | Measured | FEA | stator winding | stator core | rotor |
| 1955 | 326 | 3039 | 14.8 | 15.6 | 0.36 | 0.35 | 80 | 262 | 68 |
| 3075 | 314 | 4236 | 15.9 | 16.4 | 0.49 | 0.48 | 96 | 245 | 85 |
| 4110 | 293 | 5414 | 18.2 | 18 | 0.59 | 0.59 | 119 | 221 | 118 |

was not possible to precisely determine the electromagnetic losses in the measured machine since the exact amount of mechanical losses were unknown. Another difficulty arose from the impeller efficiency variation which was dependent upon the air pressure and flow. Therefore, the comparison between the calculated and measured data was limited.

## VI. Conclusion

This paper describes the design of an induction machine with a squirrel cage rotor for a high-speed application. It investigates the dimensioning, material, and topology selection of the rotor and its manufacturing. The mechanical machine constants,torque per rotor volume and recommended tangential stress values are analyzed for a large amount of water-cooled high-speed induction machines with solid squirrel cage rotors based on available industrial data. The typical material selection for the rotor components is presented. Suitable rotor topology solutions that allow the squirrel cage rotor to run at high rotational speeds are identified and compared.

During the case study, four rotor topologies were optimized, analyzed by mechanical calculations, and compared. According to the comparison results, the topology with two retaining rings has the highest rotor component safety factors. The electromagnetic analysis of the case study has shown that the solid rotor open slots increase the machine power factor and efficiency. Several manufacturing approaches were initially tested. Among them, two manufacturing options have demonstrated promising results. Brazing by silver brazing alloy and torch was not successful, and further investigation of this method is required. The second presented manufacturing approach is the shrink fit assembly. This method enabled construction of the designed rotor, and the detailed manufacturing steps are presented in this paper. The manufactured prototype was tested without compressor housing up to nominal speed operation in order to verify rotor behavior. For prototype testing under load conditions the test bench was used. This revealed that a comparison of the measured and calculated data was limited although rough data of the amount and distribution of electromagnetic losses was provided.

The presented research results can be utilized for squirrel cage solid rotor design and manufacturing in challenging high-speed applications.

## References

[1] A. Boglietti, C. Gerada, and A. Cavagnino, "High-speed electrical machines and drives," *IEEE Trans. Ind. Electron.*, vol. 61, no. 6, pp. 2943–2945, Jun. 2014.

[2] N. Fernando, G. Vakil, P. Arumugam, E. Amankwah, C. Gerada, and S. Bozhko, "Impact of soft magnetic material on design of high-speed permanent-magnet machines," *IEEE Trans. Ind. Electron.*, vol. 64, no. 3, pp. 2415–2423, Mar. 2017.

[3] D. Fodorean, L. Idoumghar, M. Brevilliers, P. Minciunescu, and C. Irimia, "Hybrid differential evolution algorithm employed for the optimum design of a high-speed pmsm used for ev propulsion," *IEEE Trans. Ind. Electron.*, vol. 64, no. 12, pp. 9824–9833, Dec. 2017.

[4] Z. Huang and J. Fang, "Multiphysics design and optimization of high-speed permanent-magnet electrical machines for air blower applications," *IEEE Trans. Ind. Electron.*, vol. 63, no. 5, pp. 2766–2774, May. 2016.

[5] A. Arkkio, T. Jokinen, and E. Lantto, "Induction and permanent-magnet synchronous machines for high-speed applications," in *Proc. 2005 International Conference on Electrical Machines and Systems (ICEMS)*, vol. 2, pp. 871–876, Sep. 2005.

[6] A. Smirnov, N. Uzhegov, T. Sillanpää, J. Pyrhönen, and O. P. Pyrhönen, "High-speed electrical machine with active magnetic bearing system optimization," *IEEE Trans. Ind. Electron.*, vol. 64, no. 12, pp. 9876–9885, Dec. 2017.

[7] J. Barta, N. Uzhegov, C. Ondrusek, and J. Pyrhönen, "High-speed electrical machine topology selection for the 6 kw, 120 000 rpm helium turbo-circulator," *Int. Rev. Electr. Eng. (IREE)*, vol. 11, no. 1, pp. 36–44, 2016.

[8] J. F. Gieras and J. Saari, "Performance calculation for a high-speed solid-rotor induction motor," *IEEE Trans. Ind. Electron.*, vol. 59, no. 6, pp. 2689–2700, 2012.

[9] N. Uzhegov, E. Kurvinen, J. Nerg, J. Pyrhönen, J. T. Sopanen, and S. Shirinskii, "Multidisciplinary Design Process of a 6-Slot 2-Pole High-Speed Permanent-Magnet Synchronous Machine," *IEEE Trans. Ind. Electron.*, vol. 63, no. 2, pp. 784–795, Feb. 2016.

[10] M. Ikeda, S. Sakabe, and K. Higashi, "Experimental study of high speed induction motor varying rotor core construction," *IEEE Trans. Energy Convers.*, vol. 5, no. 1, pp. 98–103, Mar. 1990.

[11] H. Zhou and F. Wang, "Comparative study on high speed induction machine with different rotor structures," in *Proc. 2007 International Conference on Electrical Machines and Systems (ICEMS)*, pp. 1009–1012, Oct. 2007.

[12] D. Gerada, A. Mebarki, N. L. Brown, C. Gerada, A. Cavagnino, and A. Boglietti, "High-speed electrical machines: Technologies, trends, and developments," *IEEE Trans. Ind. Electron.*, vol. 61, no. 6, pp. 2946–2959, Jun. 2014.

[13] J. Lähteenmäki, "Design and voltage supply of high-speed induction machines," Ph.D. dissertation, Lappeenranta University of Technology, 2002.

[14] S. Li, Y. Li, W. Choi, and B. Sarlioglu, "High-speed electric machines: Challenges and design considerations," *IEEE Trans. Transp. Electrific.*, vol. 2, no. 1, pp. 2–13, Mar. 2016.

[15] D. Gerada, A. Mebarki, N. L. Brown, K. J. Bradley, and C. Gerada, "Design aspects of high-speed high-power-density laminated-rotor induction

machines," *IEEE Trans. Ind. Electron.*, vol. 58, no. 9, pp. 4039–4047, Sep. 2011.
[16] J. Huppunen, "High-speed solid-rotor induction machine – electromagnetic calculation and design," Ph.D. dissertation, Lappeenranta University of Technology, 2004.
[17] J. Pyrhönen, J. Nerg, P. Kurronen, and U. Lauber, "High-speed, 8 mw, solid-rotor induction motor for gas compression," in *Proc. 18th International Conference on Electrical Machines (ICEM)*, pp. 1–6, Sep. 2008.
[18] W. L. Soong, G. B. Kliman, R. N. Johnson, R. A. White, and J. E. Miller, "Novel high-speed induction motor for a commercial centrifugal compressor," *IEEE Trans. Ind. Appl.*, vol. 36, no. 3, pp. 706–713, May. 2000.
[19] Y.-K. Kim, M.-C. Choi, K.-H. Suh, Y.-C. Ji, and D.-S. Wang, "High-speed induction motor development for small centrifugal compressor," in *Proc. 2001 International Conference on Electrical Machines and Systems (ICEMS)*, vol. 2, pp. 891–894, Aug. 2001.
[20] L. Papini, D. Gerada, and C. Gerada, "Development and testing aspects of high speed induction machines," in *Proc. 2016 International Conference on Electrical Machines and Systems (ICEMS)*, pp. 1–6, Nov. 2016.
[21] L. Durantay, N. Velly, J. F. Pradurat, and M. Chisholm, "New testing method for large high-speed induction motors," *IEEE Trans. Ind. Appl.*, vol. 53, no. 1, pp. 660–666, Jan. 2017.
[22] J. Barta, C. Ondrusek, P. Losak, and R. Vlach, "Design of high-speed induction machine for the 6 kw, 120 000 rpm helium turbo-circulator," in *Proc. 22th International Conference on Electrical Machines (ICEM)*, pp. 1552–1558, Sep. 2016.
[23] M. T. Caprio, V. Lelos, J. D. Herbst, and J. Upshaw, "Advanced induction motor endring design features for high speed applications," in *Proc. 17th International Conference on Electric Machines and Drives (IEMDC)*, pp. 993–998, May. 2005.
[24] T. Epskamp, B. Butz, and M. Doppelbauer, "Design and analysis of a high-speed induction machine as electric vehicle traction drive," in *Proc. 18th European Conference on Power Electronics and Applications (EPE)*, pp. 1–10, Sep. 2016.
[25] J. Pyrhönen, T. Jokinen, and V. Hrabovcova, *Design of Rotating Electrical Machines*. John Wiley & Sons, 2013.
[26] Asynchronous motor elements, 2 pole types. e+a Elektromaschinen und Antriebe AG. (2017) Accessed Aug. 29, 2017. [Online]. Available: https://www.eunda.ch
[27] Asynchronous motor elements, 2-pole elan types. e+a Elektromaschinen und Antriebe AG. (2017) Accessed Aug. 29, 2017. [Online]. Available: https://www.eunda.ch
[28] Partial motors asynchronous, 2 pole. ate antriebstechnik und entwicklungs gmbh & co. KG. (2017) Accessed Aug. 29, 2017. [Online]. Available: http://www.ate-system.de
[29] J. Hendershot and T. Miller, *Design of Brushless Permanent-magnet Machines*. Motor Design Books, 2010. [Online]. Available: https://books.google.cz/books?id=n833QwAACAAJ
[30] C. Brown, "Design for manufacturability of a high-performance induction motor rotor," Ph.D. dissertation, Massachusetts Institute of Technology, 1996.
[31] M. Centner and U. Schafer, "Optimized design of high-speed induction motors in respect of the electrical steel grade," *IEEE Trans. Ind. Electron.*, vol. 57, no. 1, pp. 288–295, Jan. 2010.
[32] M. Centner, R. Hanitsch, and U. Schafer, "Comparison of high-speed induction motors employing cobalt-iron and silicon electrical steel," in *Proc. 18th International Conference on Electrical Machines (ICEM)*, pp. 1–6, Sep. 2008.
[33] P. M. Novotny and G. E. Maurer, "Ultra high strength steel v/s titanium alloys," *Adv. Mat. & Processes*, vol. 165, no. 11, pp. 37–40, 2016.
[34] M. Caprio, V. Lelos, J. Herbst, S. Manifold, and H. Jordon, "High strength induction machine, rotor, rotor cage end ring and bar joint, rotor end ring, and related methods," *U.S. Patent Publ.*, no. US11338936, 2006.
[35] P. Beer, J. Tessaro, B. Eckels, and P. Gaberson, "High-speed motor design for gas compressor applications," in *35th Turbomachinery Symposium*, pp. 103–112, 2006.
[36] J. F. Gieras, *Advancements in Electric Machines*. Springer, Dordrecht, 2008.
[37] N. Uzhegov, J. Barta, J. Kurfurst, C. Ondrusek, and J. Pyrhönen, "Comparison of high-speed electrical motors for a turbo circulator application," *IEEE Trans. Ind. Appl.*, vol. 53, no. 5, pp. 4308–4317, Sep. 2017.

**Jan Barta** graduated with a B.Sc., M.Sc., and Ph.D. in power electrical and electronic engineering from Brno University of Technology, Brno, the Czech Republic in 2012, 2014 and 2018 respectively.

He has been working for Brno University of Technology as technical staff in research of electrical machines from 2014 to 2018. He is currently an assistant professor at the Department of Power Electrical and Electronic Engineering, Brno University of Technology. His scientific interest includes high-speed and high-efficiency electrical machines.

**Nikita Uzhegov** (M'14) received the M.Sc. and the D.Sc. degree in electrical engineering from Lappeenranta University of Technology (LUT), Lappeenranta, Finland, in 2012 and in 2016, respectively.

He has been working at LUT as a Researcher in the School of Energy Systems from 2012 to 2016. He is currently a co-founder and electrical machine designer at SpinDrive, Lappeenranta, Finland. His research mainly concerns high-speed electrical machines, design optimization, and materials used in electrical machines.

**Petr Losak** received the Ph.D. degree in applied mechanics from Brno University of Technology, Brno, Czech Republic, in 2011.

He has been working in L. K. Engineering as an Structural Analyst within period 2009 to 2012. He is currently an assistant professor at the Institute of Solid Mechanics, Mechatronics and Biomechanics, Brno University of Technology. His scientific interest includes rotordynamics, vibration analysis and stress/strain analysis.

**Ondrusek Cestmir** received the M.Sc. degree in electrical and special aircraft equipment, and the D.Sc. degree in theoretical electrical engineering from the Military Academy, Brno, Czech Republic, 1965 and 1977, respectively.

He is currently an Associate Professor at the Department of Power Electrical and Electronic Engineering, Brno University of Technology. His main research interests include electrical machines.

**Martin Mach** received Ph.D. degree in power electrical and electronic engineering from Brno University of Technology, Brno, the Czech Republic in 2016.

He is currently an Assistant Professor with the Department of Power Electrical and Electronic Engineering at the Brno University of Technology. His research interests include design and optimization of electrical machines.

**Juha Pyrhönen** (M'06, SM'17) received the Doctor of Science (D.Sc.) degree from Lappeenranta University of Technology (LUT), Finland in 1991. He became Professor of Electrical Machines and Drives in 1997 at LUT.

He is engaged in research and development of electric motors and drives. Prof. Pyrhönen has wide experience in the research and development of special electric drives for distributed power production, traction and high-speed applications. Permanent magnet materials and applying them in machines have an important role in his research.